

Inverse Biometrics: Generating Vascular Images From Binary Templates

Christof Kauba^{ID}, Simon Kirchgasser^{ID}, Vahid Mirjalili^{ID}, Andreas Uhl, *Senior Member, IEEE*, and Arun Ross^{ID}, *Senior Member, IEEE*

Abstract—In this work, we investigate the possibility of generating grayscale images of finger and hand vein patterns from their corresponding binary templates. This would allow us to determine the invertibility of vascular templates, which has implications in biometric security and privacy. The transformation from binary features to a gray-scale image is accomplished using a Pix2Pix Convolutional Neural Network (CNN). The reversibility of 6 different types of binary features is evaluated using this CNN. Further, a number of experiments are conducted using 8 distinct finger vein datasets and 3 hand vein datasets. Results indicate that (a) it is possible to reconstruct the considered vascular images from their binary templates; (b) the reconstructed images can be used for biometric recognition purposes; (c) the CNN trained on one dataset can be successfully used for reconstructing images in a different dataset (cross-dataset reconstruction); and (d) the images reconstructed from one set of features can be successfully used to extract a different set of features for biometric recognition (cross-feature-set generalization). The results of this research further underscore the need for properly securing biometric templates, even if they are of binary nature.

Index Terms—Inverse biometrics, finger vein recognition, hand vein recognition, CNN-based reconstruction, template protection.

I. INTRODUCTION

A BIOMETRIC system may be viewed as a pattern recognition system consisting of a sensor module, a feature extractor module and a comparison module [27]. The sensor module captures the biometric data; the feature extractor

Manuscript received February 6, 2021; revised April 11, 2021; accepted April 12, 2021. Date of publication April 19, 2021; date of current version December 1, 2021. This work was supported by IJCB 2020 publication: “Inverse Biometrics: Reconstructing Grayscale Finger Vein Images From Binary Features.” The work of Christof Kauba and Simon Kirchgasser was supported in part by FWF Project “Advanced Methods and Applications for Fingervein Recognition” under Grant P32201, and in part by the European Union’s Horizon 2020 Research and Innovation Program under Grant 690907 (IDENTITY). The work of Arun Ross and Vahid Mirjalili was supported by the U.S. National Science Foundation under Grant 1618518. This article was recommended for publication by Associate Editor V. Štruc upon evaluation of the reviewers’ comments. (*Christof Kauba, Simon Kirchgasser, and Vahid Mirjalili contributed equally to this work.*) (*Corresponding author: Christof Kauba.*)

Christof Kauba and Simon Kirchgasser were with Michigan State University, East Lansing, MI 48824 USA. They are now with the Department of Computer Sciences, University of Salzburg, 5020 Salzburg, Austria (e-mail: ckauba@cs.sbg.ac.at; skirch@cs.sbg.ac.at)

Vahid Mirjalili was with the Department of Computer Science and Engineering, Michigan State University, East Lansing, MI 48824 USA (e-mail: mirjalil@cse.msu.edu).

Arun Ross is with the Department of Computer Science and Engineering, Michigan State University, East Lansing, MI 48824 USA (e-mail: rossarun@cse.msu.edu).

Andreas Uhl is with the Department of Computer Science, University of Salzburg, 5020 Salzburg, Austria (e-mail: uhl@cs.sbg.ac.at).

Digital Object Identifier 10.1109/TBIM.2021.3073666

computes a set of numerical features from the data; and the comparison module inputs two feature sets and generates a match score denoting their degree of similarity or dissimilarity. The feature set that is extracted from the biometric data and stored in a database is often denoted as the feature template. Since the template is a compact and reduced representation of the input data, it is commonly assumed that the original data (e.g., image) cannot be reconstructed from the template. This has positive implications as far as the security and privacy of biometric templates are concerned [28].

However, in recent years, researchers have upended this notion and demonstrated the possibility of reverse engineering templates and reconstructing the original biometric data for fingerprint, face and iris modalities [52]. This has raised privacy and security concerns since the reconstructed image may divulge information about the individual that was not evident in the template.

In this work, we consider the problem of deducing palm and finger vein *images* from their corresponding feature *templates*. The problem is challenging since the feature templates, in this case, are *binary* in nature. Further, a number of different feature extractors have been developed resulting in different sets of binary templates. The entropy of such binary templates are very restricted compared to non-binary templates such as the ones encountered in face and fingerprint recognition.

In a previous work [30], we established the possibility of deriving finger vein images from their corresponding binary templates. In this regard, we addressed and demonstrated the following issues: (a) a suitable CNN architecture to reconstruct gray-scale images from feature-rich binary images; (b) reconstructing gray-scale finger vein images from binary templates pertaining to a single given dataset (i.e., intra-dataset reconstruction); and (c) reconstructing gray-scale finger vein images from binary templates in a dataset that was not used for training the CNN (i.e., cross-dataset reconstruction).

In this work, we extend our study to hand vein patterns. The cross-dataset (or inter-dataset) reconstruction in particular poses a security threat for biometric recognition systems that store binary templates. As there are several publicly available finger and hand vein datasets, it is possible to extract binary features from the images in these datasets and use them to train a CNN model. If this CNN model can ingest binary templates from previously unseen databases (i.e., databases or datasets that were *not* used in the training phase) and reconstruct the original images, it can lead to possible security violations. To assess the risk imposed by this attack we conducted

an inverse biometric threat assessment as proposed by [19] (IAMR) which is a recent methodology to evaluate inverse biometric approaches. These templates can be input to the trained CNN model to regenerate digital images which can then be used to extract additional information about individuals or to attack the biometric system based on finger/hand vascular patterns. For example, it may be possible to launch a presentation attack (PA) by generating a *physical* spoof artifact [57] from the digitally reconstructed image.

All in all, there are two public PA finger vein datasets, the VERA-FV Spoofing [58] and SCUT-FVD [49]. Both are based on paper printouts of the original gray scale sample images. Hence, if only the binary templates are available, a gray scale reconstruction (inversion of the templates) to generate the necessary samples for this kind of PA is essential. Moreover, all existing PAD methods for vascular pattern based biometrics are trained on gray scale samples as bona fide. Hence, a binary feature template as an input sample would be detected as an attack immediately. In order to further motivate the need of the gray scale reconstruction we evaluated the attack performance in case a binary template instead of the reconstructed gray scale image is directly used as an input to the attacked system.

This research is based on our previous work [30], where we showed that it is possible to reconstruct gray-scale *finger* vein images from their binary feature templates. This work extends our previous research by exploring the invertibility of 6 different types of binary templates corresponding to 8 different finger vein datasets as well as 3 different hand vein datasets. While 7 of the 8 finger vein datasets were explored in [30], the hand vein biometric modality is investigated for the first time in the current work. In contrast to finger vein images, hand vein data can be considered more challenging; on one hand, they have less fine-structured vascular pattern information and on the other hand they exhibit noise such as skin texture information, wrinkles and hair. Furthermore, in our previous work, the performance on the UTFVP finger vein dataset was inferior compared to the other datasets. This issue has been addressed in the current paper, resulting in markedly improved performance on this dataset.

The remainder of the paper is organized as follows: Section II provides an overview on related work in biometric image reconstruction from templates. Section III gives a short introduction to finger vein biometrics and describes the utilized datasets. Section IV gives a short introduction to hand vein biometrics and describes the utilized datasets. Section V discusses the recognition process for hand and vein biometrics. The proposed CNN-based reconstruction approach is explained in Section VI. Section VII presents the experimental protocol used and discusses the results, including the baseline performance, the use of the binary template as attack sample, the intra- as well as the inter-dataset reconstruction evaluation and the IAMR assessment. Conclusions and future work are given in Section VIII.

II. RELATED WORK

Image-to-Image Translation: The phrase “image-to-image translation” was first coined in [26], and defined as a class of

TABLE I
SUMMARY OF APPROACHES FOR INVERSE BIOMETRICS IN THE CONTEXT OF HAND GEOMETRY, FINGERPRINTS, IRIS, AND FACE MODALITIES

approach	modality	template type
Gomez-Barrero <i>et.al.</i> [20]	hand geometry	geometric information
Ross <i>et.al.</i> [52], [53]	fingerprints	minutiae
Feng and Jain [16], [17]	fingerprints	minutiae
Cappelli <i>et.al.</i> [8], [9]	fingerprints	minutiae + additional information
Cao and Jain [7]	fingerprints	ridge and phase structure
Galbally <i>et.al.</i> [18]	iris	IrisCode
Venugopalan <i>et.al.</i> [61]	iris	IrisCode
Yan <i>et.al.</i> [63]	face	facial appearance attributes
Mai <i>et.al.</i> [42]	face	DeepFace template

computer vision tasks where the goal is to learn a mapping to translate images from domain A to domain B. Image-to-image translation tasks can be divided into two categories: paired and unpaired. In paired translation [26], [62], the training data contains *aligned* input and output images. Such tasks include colorizing grayscale images [25], [38], semantic segmentation [40], and reconstructing objects from edge maps [43]. In unpaired translation, the alignment between inputs and outputs in the training data is not defined [68]. An example would be the transfer of facial attributes [12], [13], [23]. Lack of alignment makes unpaired translation an unsupervised task, and to handle the challenges of unsupervised settings, proposed methods rely on cycle-consistency and assumption of shared latent space between the two domains [68].

Convolutional neural networks have been widely used for image-to-image translation [38], [40]. Traditionally, this task was formulated as per-pixel classification. Such a treatment, however, loses the conditional dependency among output pixels given the input image [26]. Furthermore, the use of Euclidean distance results in blurry images. The Pix2Pix [26] method instead proposed a structured loss using GANs (Generative Adversarial Networks) to penalize the joint configuration of output pixels conditioned on the input image. While the use of L_2 distance in prior work resulted in blurry images, the use of L_1 distance along with GAN-loss in Pix2Pix [26] resulted in sharp and realistic outputs.

Inverse Biometrics: A recent study by Gomez-Barrero *et al.* [19] analyzed the aspect of inverse biometrics from several points of view, including a comprehensive definition of inverse biometrics and an evaluation as well as a mitigation strategy to handle this potential security threat. Thus, a two-stage experimental protocol was proposed for the evaluation of the threat posed by inverse biometric algorithms by defining four scenarios based on knowledge about the sample inversion process and the systems that should be attacked by the inverted samples. More details on the evaluation are given in Section VII-A and the results on our gray scale reconstruction are presented in Section VII-E. Furthermore, the intriguing possibility of deducing biometric images from their templates has been well explored in the context of fingerprint, iris, and face modalities. Table I summarizes the most significant work on this topic.

In the case of fingerprints, Ross *et al.* [52], [53] and Feng and Jain [16], [17] demonstrated the viability of generating fingerprint images from just the minutiae points. Cappelli *et al.* [8], [9] showed that it is possible to reconstruct

fingerprint images from standard ISO fingerprint templates that contain information beyond just minutiae points. A more recent work by Cao and Jain [7] presents an advanced approach based on prior knowledge about the fingerprint ridge and phase structure, which is encoded as a dictionary of orientation and phase patches. These dictionaries are then used to reconstruct the orientation field and ridge patterns of the fingerprint from minutiae information.

In the context of iris, Galbally *et al.* [18] utilized a probabilistic approach based on a genetic algorithm to perform iris image reconstruction from binary IrisCodes. Venugopalan and Savvides [61] developed a scheme to generate a discriminative texture pattern from an IrisCode with the purpose of embedding this pattern in a different person's iris image thereby facilitating a digital spoof attack.

In the area of face recognition, Yan *et al.* [63] utilised a generative model based on a variational auto-encoder to reconstruct face images from disentangled latent representations. Their results were promising and the reconstructed faces looked realistic. Another approach to invert face templates was presented by Mai *et al.* [42] who utilized a neighborly de-CNN (NbNet) to reconstruct face images from templates created by a deep face CNN. In contrast to other modalities like fingerprint and iris, the finger and hand vein features are extremely sparse and, hence, there is a lot less information available in the extracted binary templates. Moreover, these images usually suffer from over/underexposed areas and uneven illumination, making the vascular pattern barely visible and, in many cases, leading to broken vein lines and spurious vein lines as well.

Template Protection: This research area is closely related to inverse biometrics as successfully inverting biometric samples enables to launch presentation attacks on biometric systems. One possibility to address the security threat associated with inverting biometric templates is the application of biometric template protection (BTP). Requirements of BTP methods are specified in ISO/IEC Standard 24745 [1] and 30136 [2], namely, *non-invertibility or irreversibility, revocability or renewability, non-linkability or unlinkability and performance preservation*. Three main BTP categories can be defined [6]: (1) cancellable biometrics (CB) [47], (2) biometric cryptosystems (BCS) [50], and (3) biometrics in the encrypted domain (BED) [5].

In the context of vascular biometrics several recent approaches exist that can be applied to protect the biometric template. We will not discuss them here in detail, but the interested reader is referred to [35], [48] for studies on CB and [10], [15], [22], [64] where various BCS are proposed and evaluated.

III. FINGER VEIN RECOGNITION

Vascular biometrics, which include finger as well as hand vein biometrics, deal with person-specific characteristic patterns formed by the human blood vessels. As these vessels are located inside the human body this biometric modality is based on an internal biometric trait, similar like retina biometrics. The vascular patterns can be made visible due to the hemoglobin contained in the blood. This iron-containing

TABLE II
ALL CONSIDERED FINGER VEIN DATASETS, INCLUDING DATASET NAME, VIEW (DORSAL OR PALMAR; DOR/PAL), NUMBER OF SUBJECTS (SUBJ), NUMBER OF FINGERS PER SUBJECT (FGS), TOTAL NUMBER OF IMAGES (IMGS), NUMBER OF SESSIONS (S) AND IMAGE SIZE

dataset name	dor/pal	subj	fgs	imgs	s	image size
FV-USM [3]	palmar	123	4	5940	2	640x480
MMCBNU_6000 [41]	palmar	100	6	6000	1	640x480
UTFVP [59]	palmar	60	6	1440	2	672x380
PV-FV3 Dors [31]	dorsal	60	6	3600	1	1280x1024
PV-FV3 Palm [31]	palmar	60	6	3600	1	1280x1024
SDUMLA [65]	palmar	106	6	3816	1	320x240

protein complex is not only responsible for the red color of human blood but also has a higher light absorption coefficient in the near-infrared (NIR) spectrum than the surrounding tissue. As consequence, the vessel area becomes visible in captured images as dark lines if NIR illumination and NIR sensitive cameras [60] are utilized. There are two common set-ups for the image sensor and light source: reflected light, where the image sensor and light source are positioned next to each other on the same side of the finger/hand. The NIR light enters the tissue from the same side as it is emitted again. In light transmission set-up, the light source and image sensor are positioned on opposite sides of the finger/hand and the NIR light enters the tissue at one side, travels through the whole finger/hand and exits on the opposite side where it is captured by the image sensor. In order to ensure a consistent feature extraction, it is beneficial to extract the person-specific characteristics from a region of interest (ROI, which is a specific part of the captured image).

A. Utilized Finger Vein Datasets

The utilized finger vein datasets and their characteristics are summarized in Table II and described in the following.

FVUSM [3]: Contains 5904 palmar finger vein images, exhibiting a resolution of 640×480 pixels, acquired from 123 subjects. All of them participated in 2 acquisition sessions where each time 4 fingers per subject and 6 images per finger were captured by a custom built capturing device consisting of 850 nm LEDs, an NIR-pass filter and a Sony PSEye camera.

MMCBNU_6000 [41]: The 6000 palmar light transmission finger vein images, exhibiting a resolution of 640×480 pixels, contained in this dataset were acquired from 100 subjects. From all of them 6 fingers per subject and 10 images per finger were captured in a single session utilizing a capturing system based on 850 nm LEDs and a modified webcam. The applied modification replaces the NIR blocking filter by an 850 nm NIR-pass one.

UTFVP [59]: Contains 1440 palmar light transmission finger vein images, exhibiting a resolution of 672×380 pixels, acquired from 60 subjects. From all of them 6 fingers per subject and 4 images per finger were captured in a single session utilizing a custom built capturing device using 850 nm LEDs, a 930 nm NIR-pass filter and a C-Cam BCi5 monochrome camera.

PLUSVein-FV3 [31]: This dataset contains 4 subsets of dorsal and palmar light transmission finger vein images:

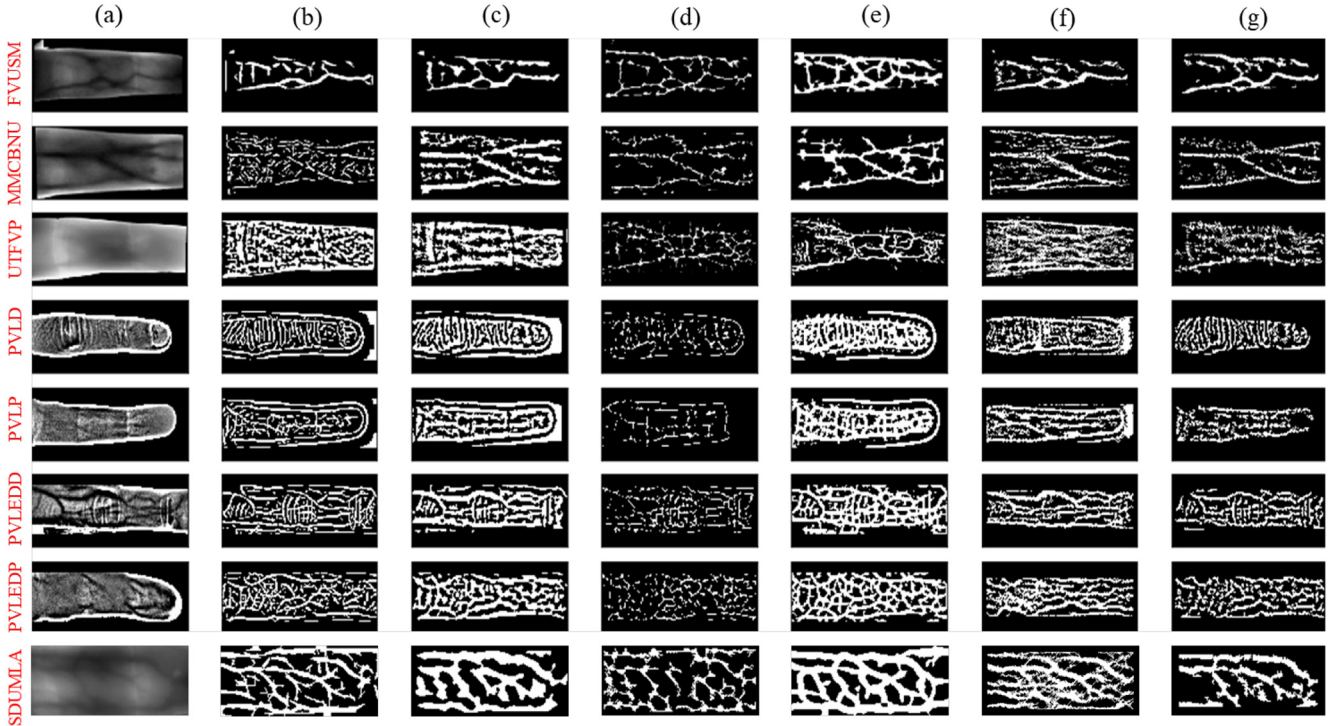


Fig. 1. Examples of pre-processed finger vein images (a) and the corresponding extracted features (using the (b) GF, (c) IUWT, (d) MC, (e) PC, (f) RLT and (g) WLD methods) from all 8 finger vein datasets considered in this study.

Laser Dorsal (PVLD), Laser Palmar (PVLP), LED Dorsal (PVLEDD), LED Palmar (PVLEDP). Each of these subsets contains 1800 images, which exhibit a resolution of 200×750 pixels, acquired from 60 subjects. From all of them 6 fingers per subject and 5 images per finger have been acquired in a single session. The data acquisition was done by the use of two different capturing devices based on a IDS UI-ML1240-NIR camera with an 850nm NIR-pass filter. Both systems differ due to the utilized illumination modules: The first one is based on NIR LEDs with a peak wavelength of 850 nm, whereas the second one is based on NIR laser modules with a peak wavelength of 808 nm.

SDUMLA [65]: Contains palmar finger vein images of left/right index, middle and ring finger from 106 subjects. From all of them 6 fingers per subject and 6 images per finger have been acquired in a single session. This results in a total of 3816 images, each exhibiting a resolution of 320×240 pixels.

Fig. 1 shows example images from each of the 8 considered finger vein datasets. Each dataset exhibits distinct characteristics in terms of extracted ROI, varying vein widths, vein clarity and contrast, as well as changes in background noise (some images have a uniform background whereas there are some artifacts of the capturing device visible in others). All these varying characteristics increase the reconstruction's difficulty as there is a greater variety in the training and testing data.

IV. HAND VEIN RECOGNITION

Hand vein biometrics is closely related to finger vein biometrics. Thus, most relevant characteristics are shared, e.g., the

TABLE III
ALL CONSIDERED HAND VEIN DATASETS, INCLUDING DATASET NAME, VIEW (DORSAL OR PALMAR; DOR/PAL), NUMBER OF SUBJECTS (SUBJ), NUMBER OF FINGERS PER SUBJECT (FGS), TOTAL NUMBER OF IMAGES (IMGS), NUMBER OF SESSIONS (S) AND IMAGE SIZE

dataset name	dor/pal	subj	fgs	imgs	s	image size
CIE-HV [29]	palmar	50	12	1200	3	1280x960
PROTECT-HV [54]	dorsal	40	5	400	1	384x384
VERA [56]	palmar	110	5	2200	2	580x680

used patterns are formed by the blood vessels located inside the human body. The sole difference is the specific region in the hand from where the biometric trait is captured. In hand vein biometrics, the NIR images containing the vascular patterns are acquired from the dorsal or palmar side of the hand instead of the finger region as done in finger vein biometrics. Although a bigger area can be used to extract biometric information from the hand region, there are more skin wrinkles and skin hair on the hand than on the finger, which are prone to be mistakenly detected as blood vessels and potentially impacting the recognition performance.

A. Utilized Hand Vein Datasets

The utilized hand vein datasets and their characteristics are summarized in Table III and described in the following.

CIE-HV [29]: Contains 1200 palmar hand vein images captured using reflected light illumination. The images have been acquired for left and right hand in three sessions. All of the images exhibit a resolution of 1280×960 pixels. The acquisition system was made up of a low cost USB camera in combination with IR emitting diodes.

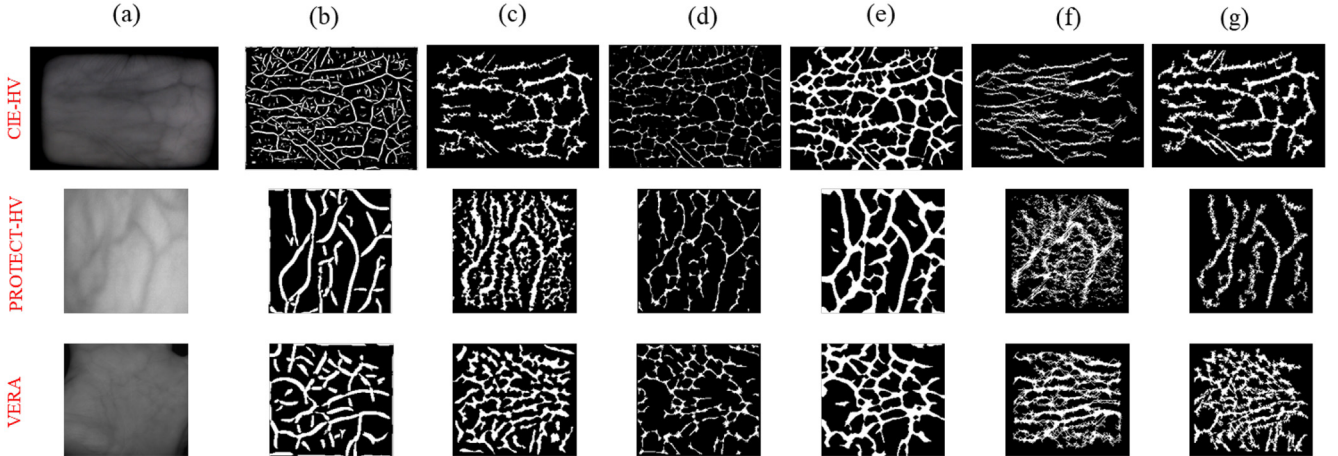


Fig. 2. Examples of original images (a) and the corresponding extracted features (using the (b) GF, (c) IUWT, (d) MC, (e) PC, (f) RLT and (g) WLD methods) from the 3 hand vein datasets considered in this study.

PROTECT-HV [54]: Contains two subsets of left and right dorsal hand vein images, acquired from 40 subjects, 5 images per hand. All images exhibit a resolution of 384×384 pixels and were captured using a reflected illuminator equipped with NIR LEDs with a peak wavelength of 950 nm. The capturing device is similar to one used for the PLUSVein-FV3 images, an IDS UI-ML1240-NIR camera with an 950 nm NIR-pass filter.

VERA [56]: Contains 2200 palmar hand vein images of both hands captured using reflected light illumination in two different sessions. The images with a resolution of 580×680 pixels were acquired by the application of an Imaging Source camera, containing a Sony ICX618 sensor and a NIR illumination of LEDs using a wavelength of 940 nm.

Fig. 2 shows example images from each of the 3 considered hand vein datasets. Similar to the finger vein datasets depicted in Fig. 1 a great variety of changes among the various images as well as vascular pattern characteristics can be detected, which is expected to increase the difficulty of the reconstruction task for the hand vein images as well. For further information on all utilized finger and hand vein datasets and the biometric capturing devices used, the interested reader is referred to [33] and [32], which include an overview and details about many of the currently available hand and finger vein datasets as well as the utilized capturing devices.

V. RECOGNITION PROCESS

The usual biometric recognition process consists of data acquisition and data processing. The first one is not described as we use already acquired data. The latter one consists of the pre-processing module, the feature extractor, the biometric template database, the comparison module and the final decision module, which are described in the following.

A. Pre-Processing

The acquired vascular images contain the finger or hand region of a subject's hand as well as the background. For the subsequent recognition process, only the finger or hand region is of interest. Thus, this area or ROI needs to be extracted

in a first step. In case finger vein images are processed, a finger outline detector [39] is applied followed by a rotational and vertical alignment of the finger [24]. If hand vein images are processed a square area centered at the hand's center of mass is extracted where the square's size depends on the hand's outline defined by four points which are detected at the middle distance between the single fingers. Afterwards, the visibility of the vein pattern is enhanced by applying **High Frequency Emphasis Filtering** (HFE) [67], **Circular Gabor Filter** (CGF) [66], **CLAHE** (local histogram equalisation) [69] as well as **Speeded Up Adaptive Contrast Enhancement** (SUACE) [4].

B. Feature Extraction Methods

Various possibilities exist for feature extraction in vascular biometrics. We selected six different template generation methods which aim to separate the gray-scale vascular patterns from the background, resulting in a binary vein template (i.e., a binary output image): Gabor Filter (**GF** [36]), Isotropic Undecimated Wavelet Transform (**IUWT** [55]), Maximum Curvature (**MC** [45]), Principal Curvature (**PC** [11]), Repeated Line Tracking (**RLT** [46]), and Wide Line Detector (**WLD** [24]). All of them can be applied to finger as well as hand vein images, respectively. Further details regarding these methods are given in [34]. Examples of binary output images are shown in Fig. 1 and Fig. 2 for finger vein examples and for hand vein images, respectively.

C. Comparison and Final Decision

All extracted features are binary representations of the vein patterns and are compared using a template comparison technique as suggested by Miura *et al.* [46]. The maximum correlation value, calculated between the input template and its x- and y-direction shifted and rotated versions of the reference template, is used as a comparison score. To decide if comparison is genuine or impostor, a pre-defined threshold is used. If the comparison score is above the threshold it is genuine, and otherwise it is deemed to be an impostor one.

VI. CNN-BASED GRAY-SCALE IMAGE RECONSTRUCTION

When reconstructing images from their binary patterns, the alignment between the input (i.e., binary pattern) and the output (i.e., vein image) is available during training. So the task is a paired image-to-image translation, where the source domain A is the concatenated binary patterns and the target domain B is the vein image. In order to determine a suitable method for performing this task, we have to account for the following factors: (a) the image translation technique has to operate on binary images; (b) the output gray-scale image has to exhibit good contrast between the veins and the background; (c) the method has to account for intra-class variations, as multiple binary templates of the same hand or finger may exhibit some differences; and (d) the method has to preserve identity information in the generated outputs. While a regular GAN can be used for this purpose, it would need additional supervision in order to generate the fine vascular structure of the hand or finger. A conditional GAN (cGAN), however, can assist in this endeavour since it learns a *conditional* generative model of the input data, i.e., it relies on the image statistics of the input domain being considered. However, we also need the cGAN to focus on certain regions in the input where discriminatory information is present. In particular, it has to account for the sparsity in the template. This highlights the need for a discriminator that accounts for local statistics (besides the global structure). This means, a pixel-wise loss function may not be suitable and a more sophisticated loss function based on the discriminator has to be used. The discriminator of the GAN, as will be described below, allows for the generation of better contrast images.

Therefore, we adapted the Pix2Pix model [26], and tuned it for this work. The architectures of the generator and discriminator are shown in Fig. 3. As in the original Pix2Pix model [26], the generator uses a U-net architecture [51] with skip connections between the down-sampling and upsampling convolution blocks. The input to the generator are binary feature patterns denoted with F , that were previously extracted from vein image I . The input features F are concatenated along their channel dimension to preserve the alignment of the inputs with the output I . The output of the generator denoted with $G(F)$ is a gray-scale vein image, reconstructed from the five input binary patterns. Down-sampling the input is performed using convolution with kernel size 3×3 and stride of 2, while increasing the number of feature maps by a factor of 2. After the bottleneck layer, four upsampling blocks using transpose convolution with kernel size 4×4 and stride 2 are followed. Finally, the last convolution layer uses kernel size 1×1 , followed by Tanh activation.

The discriminator is designed to receive binary patterns F fused with the original vein image I or the reconstructed image $\hat{I} = G(F)$, and the objective is to classify each patch of the input vein image as real or synthesized, conditioned on the aligned patch of binary patterns. Thereby forming a patchwise conditional discriminator, and is denoted by $D(I|F)$ for real input images, or $D(G(F)|F)$ for images that are reconstructed by the generator. The architecture of the discriminator is shown in Fig. 3, where the input has 6 channels (i.e., 5 binary features

F concatenated with gray-scale vein image I or \hat{I}). The discriminator uses four convolution layers with kernel size 3×3 and stride 2 for down-sampling the feature maps. Finally, the Sigmoid activation is used to get probabilities of each patch as real or synthesized.

A. Loss Function for Training the Model

For the generator, we use L_1 loss to penalize the per-pixel differences of the reconstructed and target, $L_G^{Rec} = \|G(F) - I\|_1$. Furthermore, the generator is penalized with a GAN-loss with the objective of making the reconstructed outputs indistinguishable from the targets. For this, we use a negative log-likelihood loss using the probabilities computed by our discriminator,

$$L_G^{GAN} = \frac{1}{n} \sum \log[1 - D(G(F)|F)], \quad (1)$$

where, n is the number of patches in the output of the discriminator.

The total loss for the generator is the weighted sum of the per-pixel L_1 loss:

$$L_G = \lambda_{Rec} L_G^{Rec} + L_G^{GAN}, \quad (2)$$

where, λ_{Rec} is the coefficient for balancing the reconstruction and the GAN-loss.

For the discriminator, we use the non-saturating GAN loss as designed in [21], which contains two terms, first term is to penalize the mis-classification of the patches in a real image:

$$L_D^{real} = \sum -\log[D(I|F)], \quad (3)$$

and the second term accounts for the mis-classification of synthesized images:

$$L_D^{fake} = \sum -\log[1 - D(G(F)|F)]. \quad (4)$$

The total loss for the discriminator is the sum of these two components: $L_D = \frac{1}{2}(L_D^{real} + L_D^{fake})$.

VII. EXPERIMENTAL EVALUATION

In the following, the experimental set-up, including the recognition process, the evaluation protocol and parameters, as well as the obtained results are presented.

A. Recognition Process and Protocol

For the finger- and hand-vein feature extraction and evaluation we utilized the publicly available PLUS OpenVein Tool-Kit.¹ This tool-kit includes all six feature extraction methods (GF, IUWT, MC, PC, RLT and WLD) as well as the necessary pre-processing and comparison schemes [34]. In order to assess the reconstruction performance of our proposed CNN architecture we evaluate the recognition performance by comparing the binary feature templates extracted from the reconstructed samples against the templates extracted from the original ones.

Training and evaluation protocol: For training the model, the coefficient λ_{Rec} in the generator's loss was set to 100.

¹Publicly available at: <http://www.wavelab.at/sources/OpenVein-Toolkit>.

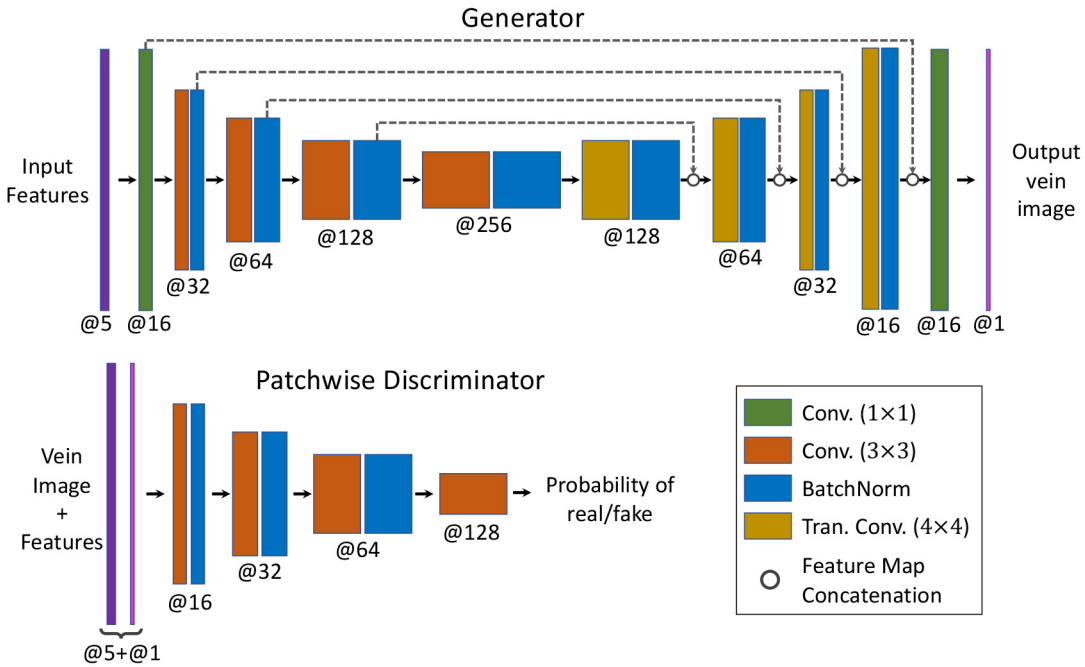


Fig. 3. The architecture of the generator and discriminator networks used in the proposed Pix2Pix model for reconstructing vein images from 5 selected binary features. The generator receives a 5-channel input and synthesizes a single-channel vein image. The discriminator receives both features and the vein image, and computes the probability of each 16×16 input patch being real or synthesized.

Adam optimizer with learning rate of $2e - 4$ was used for both the generator and discriminator networks. The models were trained for 100 epochs with a batch size of 2. All the images and features were resized to 256×256 , and normalized to the range $[-1, 1]$.

In order to show the efficacy of our reconstruction with regard to splitting and utilizing the training data, we designed two separate experiments. First, conducted **intra-dataset** experiments, where the training data from each dataset were partitioned into 5 *subject-disjoint* folds. In this set of experiments, we trained 5 models independently using 4 training folds, and the trained models were used to reconstruct the vascular images in the remaining fold. The performance for each dataset is averaged over the performance of each evaluation fold.

In the second set of experiments, rather than training models and evaluating them on the same dataset, we conducted **inter-dataset** training and evaluation, where each dataset is used for evaluation of the models that were trained on any of the other datasets. We use the term “target” to denote the dataset that was used for evaluation, and the term “source” to denote the dataset used for training the model. First, we trained the models using 100 epochs on the source datasets. Then, in order to transfer the trained models to the target dataset for evaluation, we further split the target dataset into 5 folds in a subject-disjoint manner, and used one fold for fine-tuning, and the remaining 4 folds for evaluation. This is repeated for each fold, resulting in 5 fold which can be used for the performance evaluation. We performed a total of 20 fine-tuning epochs, in which we combined the original training dataset and the fine-tuning portion of the data. After each epoch, the samples in the fine-tuning portion were oversampled by a factor of 1.1.

Finally, the last two epochs only contained the fine-tuning portion. This fine-tuning scheme was designed to gradually adapt the trained models from source to target dataset, and capture the latent characteristics of the target dataset. All but one feature type were used for training and the remaining one for reconstruction.

Inverse Biometric Threat Assessment (IAMR): Gomez-Barrero *et al.* [19] proposed a methodology to evaluate inverse biometrics approaches and the risk they pose to the attacked applications. Their method can be used to assess the performance of the inverse biometric algorithm as well as to assess the vulnerability of a given system to this threat. For the evaluation they defined different levels of knowledge needed by the inverse biometric approach: (1) template format, (2) similarity scores, (3) similarity scores and comparison function and (4) feature extraction method. These knowledge levels influence the level of threat posed by the inverse biometric method while (1) means least knowledge needed and highest threat posed. In addition to the knowledge levels, they introduced four evaluation scenarios based on the selection of the samples and the selection of the systems for the development and validation stage: (1) same samples, same systems (2) different samples, same systems, (3) same samples, different systems and (4) different samples, different systems. Case (1) poses the least threat as it needs the same samples and the same system for development and evaluation, while case (4) poses the highest threat as a successful attack works with different systems and samples (most general case). If the focus is on assessing the inverse biometrics algorithm, case (3) and (4) should be used while if the focus is on assessing the recognition system, case (1) and (2) should be considered. To quantify

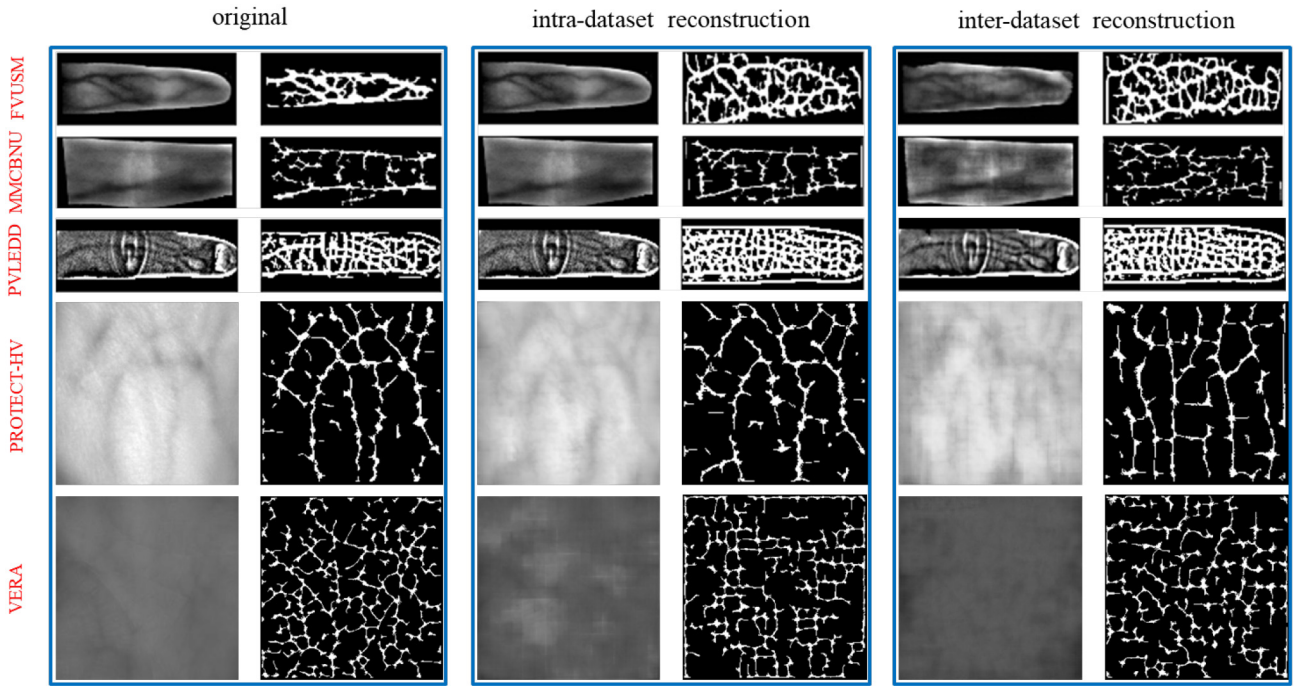


Fig. 4. Examples of reconstructed vein images and the corresponding binary templates computed using the PC feature extractor (so training was done using the remaining 5 feature sets). The inter-dataset reconstructions in the first 3 rows were obtained by pre-training the CNN model on the PVLEDP dataset, while the reconstructions in the last two rows were obtained by pre-training on the VERA and PROTECT-HV dataset, respectively.

the threat level or the performance of the inverse biometric, they introduced an inversion metric, the so called Inversion Attack Match Rate (IAMR). The IAMR evaluated the expected probability that a reconstructed sample gains access to the system at a given operating point and is defined as follows:

$$IAMR = \frac{1}{M} \sum_{m=1}^M \left\{ \max_{n \leq N} (S_m^n) > \delta \right\}$$

where M is the number of subjects being attacked, N is the number of reconstructed samples per bona-fide sample, S_m^n is the similarity score of the n -th reconstructed sample of the m -th subject and δ is the verification threshold. The verification threshold is set for desired levels of the false match rate (FMR) where the system is to be evaluated (suggested FMRs are: 0.1%, 0.05% and 0.01%).

As we are interested in evaluating the inverse biometrics algorithm itself, we chose the following evaluation framework:

- Knowledge required about the development system: template format and type of feature extraction method (needs to be binary), but no particular details about the feature extraction method.
- Samples selection: same development and validation samples (S3) as well as different development and validation samples (S4) with $N = 5$.
- System selection: different development and evaluation system (cross-feature type evaluation).

B. Baseline Results

The baseline recognition performance results for the considered finger vein samples are presented in Table IV

while the results corresponding to the original hand vein samples are presented in Table V. We use two performance metrics to measure the recognition accuracy: the equal error rate (EER) and the FMR1000 (the lowest false non match rate (FNMR) at a false match rate (FMR) $\leq 0.1\%$). The baseline performance was calculated by utilizing original finger as well as original hand vein images as provided by each dataset and the OpenVein Tool-kit's default parameters for the respective datasets.

The MC method results in the best performance values in five of the eight finger vein datasets, while the PC, WLD and IUWT methods performed best once each. Recognition performance is the best on the PLUSVein-FV3 subsets (PVLD, PVLEDD, PVLEDP) followed by UTFVP, PVLP, MMCNU and FVUSM datasets. The worst baseline performance can be observed assessing the recognition system on SDUMLA finger vein samples.

In contrast to the baseline performance obtained on the finger vein datasets, there is no clear trend on the hand vein datasets. For each of the three considered datasets a different feature extraction method resulted in the best performance. Overall, the best baseline performance is on the PROTECT-HV dataset using RLT as the feature extraction method, followed by VERA and CIE-HV. For both vascular biometric modalities the full comprehensive set of results, including the reconstruction experiments, are provided on our website² where ROC and DET plots for each dataset/experiment are available.

²<http://www.wavelab.at/sources/Kaub20b/>

TABLE IV

FINGER VEIN - BASELINE RECOGNITION PERFORMANCE (%). THE BEST RESULT FOR EACH FEATURE EXTRACTION METHOD PER FV DATASET IS HIGHLIGHTED IN **BOLD** NUMBERS. THE OVERALL BEST RECOGNITION PERFORMANCE IS ACHIEVED ON PVLEDD. THE LAST COLUMN AND ROW REPRESENT THE AVERAGE VALUES PER DATASET AND FEATURE TYPE, RESPECTIVELY

eval. method	Baseline Performance (%)						
	GF	IUWT	MC	PC	RLT	WLD	avg.
FVUSM							
EER	3.98	6.84	2.59	4.81	6.34	4.62	4.86
\bar{FMR}_{1000}	0.96	0.99	0.85	0.99	0.98	0.99	0.96
MMCBNU							
EER	5.57	2.37	0.97	0.81	5.74	1.65	2.90
\bar{FMR}_{1000}	0.91	0.86	0.54	0.46	0.95	0.76	0.75
UTFVP							
EER	0.77	0.77	0.36	0.56	2.10	0.72	0.88
\bar{FMR}_{1000}	1.33	1.28	0.51	0.92	4.05	1.28	1.56
PVLID							
EER	0.44	0.24	0.36	0.52	0.27	0.11	0.32
\bar{FMR}_{1000}	0.05	0.01	0.04	0.21	0.07	0.00	0.06
PVLIP							
EER	1.08	0.70	2.02	1.58	1.41	1.97	1.46
\bar{FMR}_{1000}	0.52	0.20	0.99	0.71	0.81	0.99	0.70
PVLEDD							
EER	0.08	0.11	0.00	0.08	0.42	0.05	0.12
\bar{FMR}_{1000}	0.00	0.00	0.00	0.00	0.13	0.00	0.02
PVLEDP							
EER	0.39	0.70	0.28	0.44	0.47	0.36	0.44
\bar{FMR}_{1000}	0.97	0.72	0.60	0.14	0.95	0.00	0.56
SDUMLA							
EER	10.07	6.86	5.11	5.22	14.61	8.67	8.42
\bar{FMR}_{1000}	22.54	12.65	8.82	9.36	22.22	19.58	15.86
avg. EER	2.79	2.32	1.46	1.75	3.91	2.26	2.41
avg. \bar{FMR}	3.41	2.08	1.54	1.59	3.76	2.94	2.56

TABLE V

HAND VEIN - BASELINE RECOGNITION PERFORMANCE (%). THE BEST RESULT FOR EACH FEATURE EXTRACTION METHOD PER HAND VEIN DATASET IS HIGHLIGHTED IN **BOLD** NUMBERS. THE OVERALL BEST RECOGNITION PERFORMANCE IS ACHIEVED ON PROTECT-HV. THE LAST COLUMN AND ROW REPRESENT THE AVERAGE VALUES PER DATASET AND FEATURE TYPE, RESPECTIVELY

eval. method	Baseline Performance (%)						
	GF	IUWT	MC	PC	RLT	WLD	avg.
CIE-HV							
EER	3.58	4.28	3.17	3.14	5.71	2.96	3.80
\bar{FMR}_{1000}	4.74	8.42	3.51	3.56	15.72	3.90	6.64
PROTECT-HV							
EER	0.24	0.37	0.24	0.24	0.12	0.75	0.32
\bar{FMR}_{1000}	0.49	0.49	0.24	0.37	0.12	1.73	0.57
VERA							
EER	3.53	2.29	2.39	3.29	2.86	3.86	3.03
\bar{FMR}_{1000}	15.84	3.00	3.55	11.77	6.62	7.64	8.07
avg. EER	2.45	2.31	1.93	2.22	2.89	2.52	2.38
avg. \bar{FMR}	7.03	3.97	2.43	5.23	7.48	4.42	5.09

C. Results of Binary Template Based Attack

In order to motivate the introduced template inversion process, we apply a simple straight-forward attack possibility without the need to invert the binary template. The idea is to obtain a subject's template based on feature type A and use this template as a sample presented to the biometric system (in a PA) which then applies a feature extraction based on feature type B. In Fig. 5 a sample template resulting from this attack is shown. The first two images on the left side show the original templates, while the ones on the right side result from applying the feature extraction on the original binary templates instead of the original HV samples.

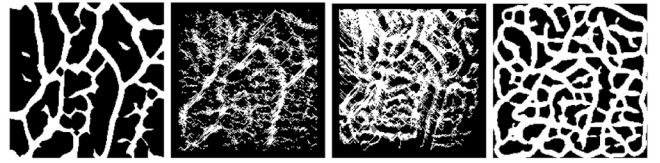


Fig. 5. Examples of cross-feature binary templates from a PROTECT-HV sample. From left to right: original PC features, original RLT features, RLT applied on the PC features and PC applied on the RLT features.

TABLE VI

EER (%) AND IAMR RESULTS OF DIRECTLY USING TEMPLATES AS NEW SAMPLES WITHOUT THE GRAY SCALE RECONSTRUCTION. GF, RLT, WLD AND PC REPRESENT THE BASELINE EER VALUES WHILE GF-RLT, GF-WLD AND PC-RLT REPRESENT THE FEATURE EXTRACTION APPLIED TO THE BASELINE TEMPLATES (RESULTS GIVEN IN **BOLD** NUMBERS). THE GENERAL LOW IAMR VALUES INDICATE THAT THE DIRECT USE OF THE TEMPLATES DOES NOT RESULT IN A SUCCESSFUL ATTACK

dataset	feat. type	EER (%)	IAMR		
			FMR	S3	S4
PVLEDD	GF	0.39	0.01%	0.0178	0.011
	RLT	0.42	0.005%	0.012	0.010
	GF-RLT	8.48	0.001%	0.007	0.006
PROTECT-HV	GF	0.24	0.01%	0.00	0.00
	WLD	0.75	0.005%	0.00	0.00
	GF-WLD	3.21	0.001%	0.00	0.00
PROTECT-HV	PC	0.24	0.01%	0.00	0.00
	RLT	0.12	0.005%	0.00	0.00
	PC-RLT	34.02	0.001%	0.00	0.00

Table VI lists corresponding results and two additional motivating example cases in terms of EER (%) and IAMR. For some combinations (PROTECT-HV GF-WLD, PVLEDD GF-RLT) the EER results suggest that this simple attack is successful (as the EER is still low when conducting this PA), while for other combinations (PROTECT-HV PC-RLT) the chance of success is rather low. The attack's efficiency depends on two factors: a) the used feature extraction methods and b) the algorithm used for template comparison. Some of the feature extraction methods tend to smooth the input and remove noise and distortions (e.g., PC applied to RLT in Fig. 5) while others introduce additional noise (e.g., RLT applied to PC in Fig. 5) which decreases the recognition performance (PROTECT-HV PC-RLT). The employed template comparison method according to Miura *et al.* [45], [46] is based on a matched pixel ratio, normalized by the number of white pixels. If the positions of the vascular lines in both templates match and they only differ in their thickness, the resulting comparison score is only slightly affected.

In contrast to the EER, the IAMR results indicate that this kind of attack poses little to no threat. For the IAMR evaluation, a pre-defined FMR level is used, i.e., the threshold to separate between genuine and imposter scores is fixed, while the threshold is variable for the EER evaluation. If the baseline performance is high (low EER), the set threshold for the IAMR will be rather high and, thus, for a successful attack, the attack samples have to achieve a high comparison score.

Especially the IAMR results confirm that this simple approach is not suitable to attack a finger/hand vein recognition system. The subsequently presented results achieved with our gray-scale reconstruction methodology show that by

TABLE VII

FINGER VEIN - INTRA-DATASET RECOGNITION PERFORMANCE (%). THE BEST RESULT FOR EACH FEATURE EXTRACTION METHOD PER DATASET IS HIGHLIGHTED IN **BOLD**. THE CNN MODEL SHOWS VERY GOOD RECONSTRUCTION PERFORMANCE IN ALL DATASETS, EXCEPT FOR UTFVP. THE LAST COLUMN AND ROW REPRESENT THE AVERAGE VALUES PER DATASET AND FEATURE TYPE, RESPECTIVELY

eval. method	intra-dataset Performance (%)						
	GF	IUWT	MC	PC	RLT	WLD	avg.
FVUSM							
EER	6.31	8.71	5.06	6.29	7.44	6.37	6.68
\bar{FMR}_{1000}	14.57	23.71	10.99	15.19	19.29	16.46	16.70
MMCNU							
EER	4.94	3.09	2.41	2.40	3.33	6.54	3.78
\bar{FMR}_{1000}	15.13	10.17	6.15	9.01	10.22	19.94	11.77
UTFVP							
EER	16.29	5.04	3.77	15.04	6.01	1.77	7.98
\bar{FMR}_{1000}	53.43	14.63	14.54	80.05	17.69	5.65	30.99
PVLD							
EER	3.44	2.63	0.00	2.90	4.50	0.00	2.24
\bar{FMR}_{1000}	12.00	7.11	0.00	7.58	14.64	0.00	6.88
PVLP							
EER	8.46	8.69	1.50	2.70	8.14	2.70	5.37
\bar{FMR}_{1000}	29.36	19.22	2.72	18.75	28.42	4.00	17.07
PVLEDD							
EER	3.61	4.92	1.53	3.14	4.55	0.00	2.96
\bar{FMR}_{1000}	13.28	15.17	3.92	7.11	16.89	0.00	9.93
SDUMLA							
EER	6.66	7.01	2.66	6.59	7.32	1.25	5.24
\bar{FMR}_{1000}	24.25	21.14	8.36	15.33	22.39	2.42	15.64
avg. EER	9.41	7.51	4.34	7.82	8.17	4.56	6.96
avg. \bar{FMR}	28.66	22.35	12.67	28.31	26.19	12.89	21.90

applying the proposed inversion, an attack becomes highly effective.

D. Results of Reconstructed Vascular Biometrics

As mentioned in Section VII-A for both vascular biometric modalities, two different evaluation protocols were considered in this work: intra-dataset and inter-dataset. The first case is probably the easier one since training as well as testing of the proposed reconstruction model was done on each of the finger and hand vein datasets independently. This allows to show that the designed CNN model is capable of generating meaningful images containing sufficient vascular pattern information that can be successfully used in the subsequent biometric recognition process. The evaluation (i.e., measuring recognition performance) in the intra-dataset case is conducted on a small subset of each dataset, since the remaining images in that dataset were needed to perform the model training. For the inter-dataset experiments, the evaluation is conducted on the entire reconstructed dataset since the training was done on the other datasets. For presenting the inter-dataset experimental results, the PVLEDD (as best representative) and FV-USM (as one worse representative) were selected for the finger vein datasets, while in the case of hand vein, we only show the results on the best performing dataset, PROTECT-HV.

1) Finger Vein Intra- and Inter-Dataset Evaluation: In Table VII, the intra-dataset recognition performance results using the finger vein datasets are presented. These results indicate that it is possible to reconstruct gray-scale finger vein images from binary templates for a single, given dataset.

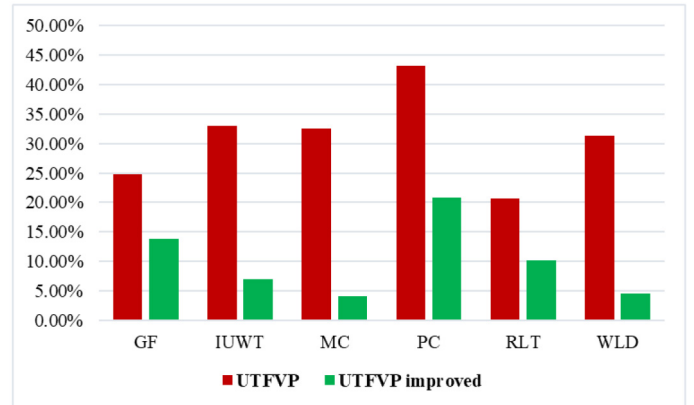


Fig. 6. Performance improvement assessing EER on the UTFVP dataset using the intra-dataset experimental protocol.

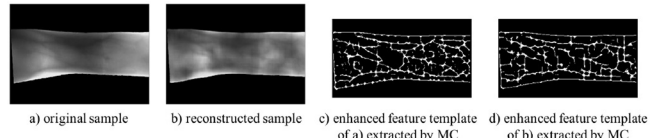


Fig. 7. Example samples of original a) and reconstructed b) UTFVP finger vein images. On the UTFVP dataset a recognition performance improvement compared to [30] is achieved by reducing the images's background information, i.e., samples a) and b), during the reconstruction experiments. This leads to smaller feature templates c), d) the comparison of which can be done with higher accuracy (see Fig. 6).

Furthermore, it also confirms that the proposed CNN architecture (see Section VI) is indeed capable of reconstructing finger vein images for an unseen feature type (cross-feature-set generalization). The reconstructed samples can be successfully used for biometric recognition. The results in Table VII show that it is possible to achieve a recognition performance which is often very close to the baseline (given in Table IV) for most datasets. Interestingly, for the PVLD and PVLEDD datasets, a performance enhancement can be seen in the intra-dataset evaluation, while for the PVLP and PVLEDP datasets only a slight degradation is observed. On the downside, the results on the UTFVP, FVUSM, MMCNU and SDUMLA datasets show a noticeable performance degradation.

In [30], it was shown that for the UTFVP dataset, the recognition performance on the reconstructed data was much lower (higher EER and \bar{FMR}_{1000}) compared to the baseline and to the results presented in this study. We have improved the recognition performance (see Fig. 6) by reducing the background information present in the images used during the reconstruction process. In Fig. 7 it can be seen that this reduction results in considerably smaller feature templates as the height of the templates is lower than the original and reconstructed images. As a consequence, the comparison of original and reconstructed feature templates can be done with higher accuracy.

According to the defined inter-dataset evaluation protocol, there are a number of different combinations possible, but we decided to show only the worst (FVUSM, see Fig. 8) and the best (PVLD, see Fig. 9).

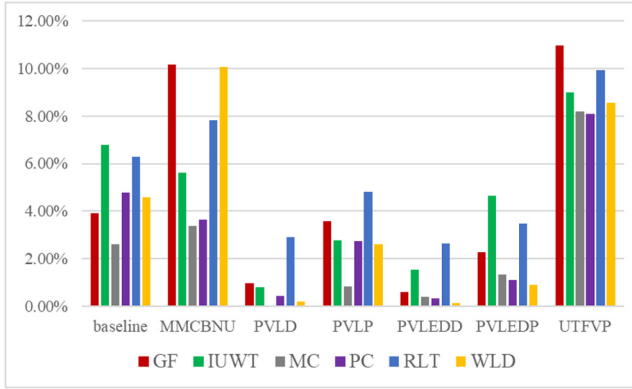


Fig. 8. Inter-dataset performance based on EER. Here, the proposed CNN model is trained only on the FVUSM dataset and tested on the other datasets, representing the overall **worst** performance obtained in the inter-dataset setting. Reconstruction on the UTFVP dataset is slightly worse compared to MMCBNU and much worse compared to the other datasets.

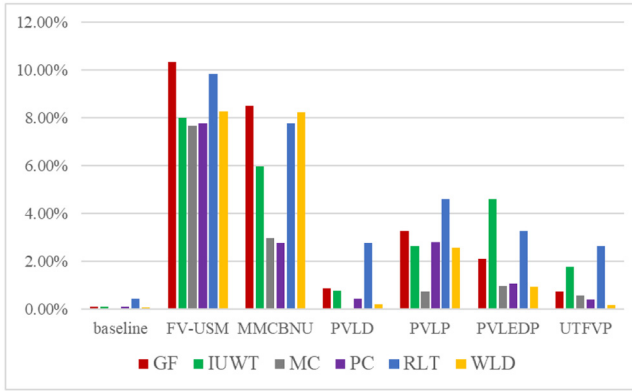


Fig. 9. Inter-dataset performance (EER). This time the CNN model is trained only on the PVLEDD dataset and tested on the other datasets, representing the overall **best** performance obtained in the inter-dataset setting. Here, the reconstruction on the FV-USM and MMCBNU datasets is by far worst compared to the others.

Apart from dataset specific variations, there is hardly any difference between the overall recognition performance trend observed on the intra-dataset evaluation and the inter-dataset experiments. As mentioned before, a comprehensive set of experiments have been conducted using almost all combinations of training and evaluation sets.

Note that the inter-dataset experiments on the SDUMLA dataset have not been included in this graphic for two reasons. First, in the intra-dataset experiments we have shown that a successful reconstruction on this dataset is possible. Second, the overall baseline and the intra-dataset recognition performance on the SDUMLA dataset is much worse compared to the other datasets. Thus, we excluded the SDUMLA specific inter-dataset evaluation results from the aforementioned figures as they would reduce the insights gained from the remaining datasets.

In Fig. 8 it can be seen that the reconstruction on the UTFVP was slightly worse compared to the MMCBNU one and both are much worse compared to the other datasets. A comparison with Fig. 9 clearly highlights that in case of UTFVP this observation is based on the dataset utilized during training. In Fig. 8

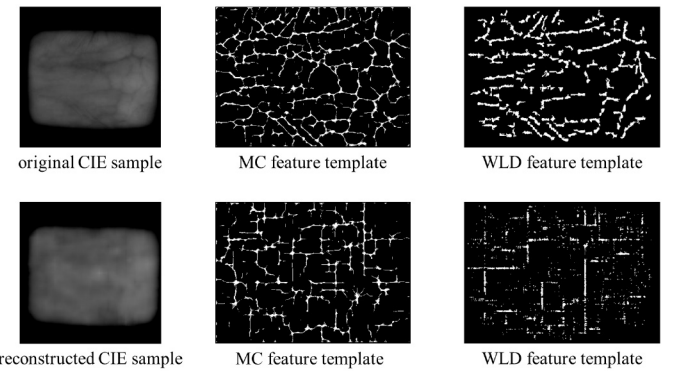


Fig. 10. Examples of original and reconstructed CIE images with their corresponding MC and WLD feature templates.

TABLE VIII
HAND VEIN - INTRA-DATASET RECOGNITION PERFORMANCE (%). THE BEST RESULT FOR EACH FEATURE EXTRACTION METHOD PER DATASET IS HIGHLIGHTED IN **BOLD**

eval. method	intra-dataset Performance (%)						avg.
	GF	IUWT	MC	PC	RLT	WLD	
PROTECT-HV							
EER	1.99	0.74	0.52	4.07	0.74	2.87	1.82
\bar{FMR}_{1000}	7.17	1.60	1.11	17.69	1.85	9.15	6.42
VERA							
EER	11.11	7.19	10.53	10.29	20.36	21.91	13.56
\bar{FMR}_{1000}	24.08	15.95	26.20	51.22	60.51	51.62	38.26
avg. EER	6.55	3.96	5.52	7.18	10.55	12.39	7.69
avg. \bar{FMR}	15.62	8.77	13.65	34.45	31.18	30.38	22.34

the EER on the UTFVP dataset is higher compared to the other datasets, while in Fig. 9 utilizing PVLEDD instead of FV-USM during training the EER is among the best. Furthermore, it can be seen that the EER for PVLD, PVLP and PVLEDD is quite stable independently from the dataset selected for training, while the recognition performance on the MMCBNU is slightly better if PVLEDD is used as training dataset.

Finally, in Fig. 11 detection error trade-off (DET) plots are shown using PVLEDD data and MC as feature type. The red line corresponds to the baseline, while the blue one depicts the intra-dataset evaluation and the green one the inter-dataset experiment (training done on MMCBNU samples). The circular point for each curve marks the EER obtained for the specific experiment. In this particular case the inter-dataset experiment was superior to the intra case (green line is below the blue line) which can be explained by the training conducted on different samples in both experiments. Note that this is an observation and not an exception and can be detected several times.

2) *Hand Vein Intra- and Inter-Dataset Evaluation:* For the hand vein evaluation we used three datasets: PROTECT-HV, CIE and VERA. The reconstruction did not work well on the CIE dataset. Fig. 10 reveals that the reconstructed images contain some grid-like pattern which distorts the actual vein pattern and leads to many spurious vein lines. We have not been able to determine the source of these gridlines. We are still investigating this issue and do not include the CIE results here.

Table VIII lists the intra-dataset evaluation results. On the PROTECT-HV, the reconstruction works well. The best

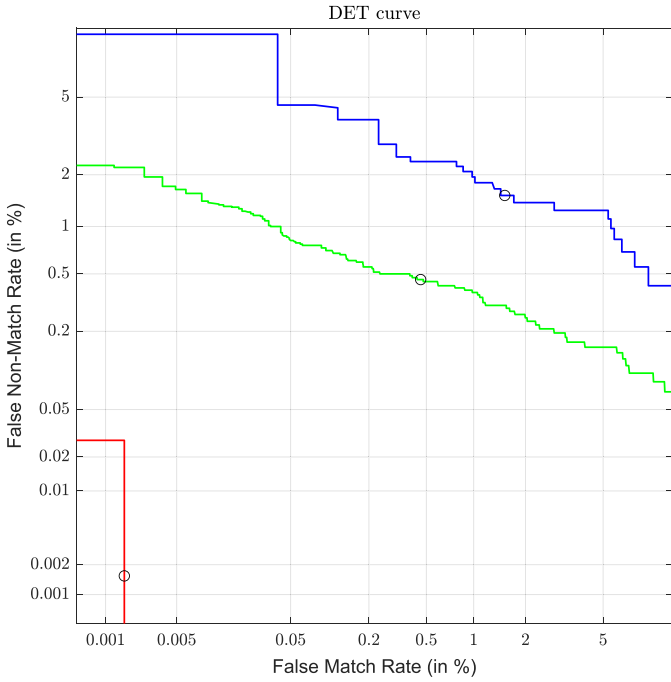


Fig. 11. DET curves (red - baseline, blue - intra-dataset, green - inter-dataset) using PVLEDD data and MC as feature type where for the the inter-dataset experiments MMCBNU samples have been utilized as training dataset.

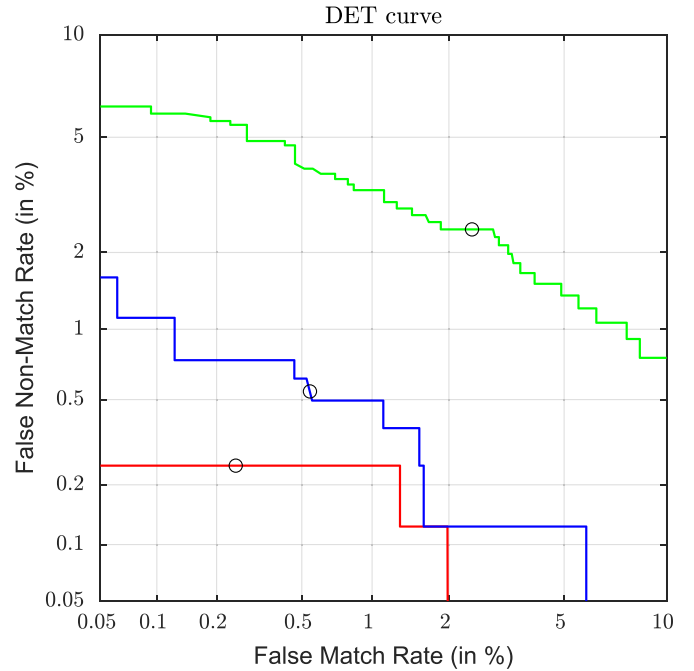


Fig. 13. DET curves (red - baseline, blue - intra-dataset, green - inter-dataset) obtained for the PROTECT-HV dataset and MC as feature type where for the the inter-dataset experiments MMCBNU samples have been utilized as training dataset.

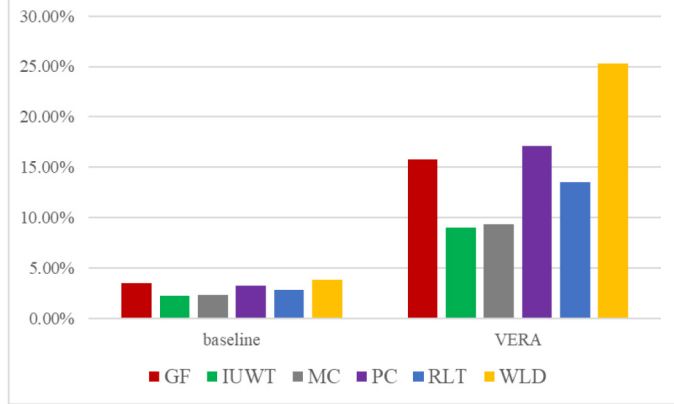


Fig. 12. Inter-dataset performance (EER). This time the CNN model is trained on the PROTECT-HV dataset and tested on the VERA dataset, representing the overall **best** performance obtained in the inter-dataset setting.

performance is achieved using MC, followed by IUWT and RLT. On the VERA dataset the reconstruction does not work that well and the performance using the reconstructed data is about 5 times worse than the baseline one (EER is 5 times higher). The best performing feature on the VERA is IUWT, followed by PC and MC.

Fig. 12 shows the performance in terms of EER for the inter-dataset reconstruction when the model is trained on PROTECT-HV and tested on the VERA dataset. Surprisingly, the inter-dataset reconstruction performs better than that of intra-dataset on the VERA dataset in two of the six feature extraction cases: MC (EER of 9.40%) and RLT (EER of 13.52%). However, the best recognition performance for this dataset is observed using IUWT (EER of 7.19%) for the intra-dataset scenario.

In general, the reconstruction on the hand vein datasets are worse compared to the finger vein ones. One reason might be the more challenging nature of the hand vein datasets; they contain (a) less vascular pattern information (only coarse structures are visible), and (b) additional artefacts in the images originating from skin texture, wrinkles and skin hair which lead to spurious vascular pattern information during feature extraction.

Finally, in Fig. 13 detection error trade-off (DET) plots are shown using PROTECT-HV data and MC as feature type. The red line corresponds to the baseline, while the blue one depicts the intra-dataset evaluation and the green one the inter-dataset experiment (training done on CIE samples). The circular point for each curve marks the EER obtained for the specific experiment. Opposed to the DET curves presented in Fig. 11 the intra-dataset experiments are always superior if compared to the inter-dataset ones.

E. Inverse Biometrics Threat Assessment Results

Table IX shows the IAMR values (ranging from 0 to 1, where 0 corresponds to no security threat at all and 1 corresponds to a perfect attack which is successful in any case, i.e., the highest possible security threat) evaluated for scenario S3 and S4 at FMR levels 0.01%, 0.005% and 0.001% averaged over all finger vein data sets per feature type. According to the IAMR results the attack was most effective for RLT in both (S3 and S4) scenarios. The values for all other feature types are still > 0.95 in any scenario and at any of the evaluated FMR levels. Hence, the inversion attack poses a severe risk for finger vein recognition systems, no matter if the same

TABLE IX

FINGER VEIN DATASETS - IAMR EVALUATION. CASES S3 AND S4 WERE EVALUATED AT DIFFERENT FMR LEVELS. THE VALUES GIVEN ARE AVERAGED PER FEATURE TYPE FOR ALL FINGER VEIN DATASETS

		IAMR					
case	FMR	GF	IUWT	MC	PC	RLT	WLD
S3	0,01%	0,987	0,986	0,991	0,986	0,999	0,988
	0,005%	0,986	0,983	0,989	0,983	0,998	0,985
	0,001%	0,981	0,975	0,985	0,977	0,995	0,977
S4	0,01%	0,975	0,978	0,983	0,974	0,986	0,976
	0,005%	0,970	0,973	0,980	0,968	0,982	0,970
	0,001%	0,958	0,959	0,971	0,953	0,973	0,954

TABLE X

HAND VEIN DATASETS - IAMR EVALUATION. CASES S3 AND S4 WERE EVALUATED AT DIFFERENT FMR LEVELS. THE VALUES GIVEN ARE AVERAGED PER FEATURE TYPE FOR ALL HAND VEIN DATASETS (EXCEPT CIE)

		IAMR					
case	FMR	GF	IUWT	MC	PC	RLT	WLD
S3	0,01%	0,907	0,911	0,909	0,906	0,392	0,402
	0,005%	0,903	0,911	0,906	0,898	0,371	0,376
	0,001%	0,878	0,911	0,904	0,845	0,329	0,335
S4	0,01%	0,868	0,888	0,873	0,842	0,381	0,377
	0,005%	0,848	0,884	0,871	0,804	0,352	0,349
	0,001%	0,769	0,877	0,862	0,708	0,293	0,302

sample from which the inverse sample is generated is stored in the database of the target system (S3) or not (S4).

Table X lists the IAMR results for the hand vein datasets, averaged over all data sets (except CIE) per feature type. The inversion attack achieves a high performance for GF, IUWT, MC and PC in both cases (S3 and S4) but especially for RLT and WLD the IAMR values are quite low, suggesting that the attack was not that successful for those feature types. In general the inversion attack is less effective for hand vein recognition than for finger vein one (see Table IX) and only poses a risk to practical systems for the GF, IUWT, MC and PC feature types.

VIII. SUMMARY AND FUTURE WORK

In this work, we used a neural network to reconstruct gray-scale finger and hand vein images from their binary templates. The proposed approach was evaluated on 8 different finger vein datasets as well as 3 hand vein datasets using 6 different types of binary templates. Following our previous work, the experiments confirmed once more the generalizability of the proposed approach across multiple datasets as well as different modalities.

In particular, we improved the reconstruction performance on the UTFVP dataset, while maintaining the same level of performance on the remaining datasets. We showed that a meaningful reconstruction is possible for hand vein datasets as well.

This strengthens our previous finding that the security and privacy of even binary templates can be compromised and that improved security constructs are of vital importance in practical applications of finger/hand vein biometrics.

Our future work will employ other types of CNN architectures and test if they are able to improve the *quality* of images generated by the reconstruction process. Furthermore, we plan

to investigate if the reconstruction performance can be maintained if the training is done on a fewer number of different binary features. So far, our approach has been only applied to feature extraction schemes resulting in binary templates. Thus, we will extend our research to other feature types, including key-point based ones (e.g., DTFPM [44]) as well as CNN based ones [14], [37].

REFERENCES

- [1] *Information Technology—Security Techniques—Biometric Information Protection*, ISO/IEC Standard 24745:2011, 2011.
- [2] *Information Technology—Performance Testing of Biometric Template Protection Schemes*, ISO/IEC Standard 30136:2018, 2018.
- [3] M. S. M. Asaari, S. A. Suandi, and B. A. Rosdi, “Fusion of band limited phase only correlation and width centroid contour distance for finger based biometrics,” *Expert Syst. Appl.*, vol. 41, no. 7, pp. 3367–3382, 2014.
- [4] A. M. R. R. Bandara, K. A. S. H. Kulathilake, and P. W. G. R. M. P. B. Giragama, “Super-efficient spatially adaptive contrast enhancement algorithm for superficial vein imaging,” in *Proc. IEEE Int. Conf. Ind. Inf. Syst. (ICIIS)*, Dec. 2017, pp. 1–6.
- [5] J. Bringer, H. Chabanne, and A. Patey, “Privacy-preserving biometric identification using secure multiparty computation: An overview and recent trends,” *IEEE Signal Process. Mag.*, vol. 30, no. 2, pp. 42–52, Mar. 2013.
- [6] P. Campisi, *Security and Privacy in Biometrics*, vol. 24. London, U.K.: Springer, 2013.
- [7] K. Cao and A. K. Jain, “Learning fingerprint reconstruction: From minutiae to image,” *IEEE Trans. Inf. Forensics Security*, vol. 10, pp. 104–117, 2015.
- [8] R. Cappelli, A. Lumini, D. Maio, and D. Maltoni, “Can fingerprints be reconstructed from ISO templates?” in *Proc. 9th Int. Conf. Control Autom. Robot. Vis.*, 2006, pp. 1–6.
- [9] R. Cappelli, D. Maio, A. Lumini, and D. Maltoni, “Fingerprint image reconstruction from standard templates,” *IEEE Trans. Pattern Anal. Mach. Intell.*, vol. 29, no. 9, pp. 1489–1503, Sep. 2007.
- [10] J. Chavez-Galaviz, J. Ruiz-Rojas, and A. Garcia-Gonzalez, “Embedded biometric cryptosystem based on finger vein patterns,” in *Proc. 12th Int. Conf. Electr. Eng. Comput. Sci. Autom. Control*, 2015, pp. 1–6.
- [11] J. H. Choi, W. Song, T. Kim, S.-R. Lee, and H. C. Kim, “Finger vein extraction using gradient normalization and principal curvature,” in *Proc. IS T/SPIE Electron. Imag.*, 2009, Art. no. 725111.
- [12] Y. Choi, M. Choi, M. Kim, J.-W. Ha, S. Kim, and J. Choo, “StarGAN: Unified generative adversarial networks for multi-domain image-to-image translation,” in *Proc. IEEE Conf. Comput. Vis. Pattern Recognit.*, 2018, pp. 8789–8797.
- [13] Y. Choi, Y. Uh, J. Yoo, and J.-W. Ha, “StarGAN v2: Diverse image synthesis for multiple domains,” in *Proc. IEEE/CVF Conf. Comput. Vis. Pattern Recognit.*, 2020, pp. 8188–8197.
- [14] R. Das, E. Piciucco, E. Maiorana, and P. Campisi, “Convolutional neural network for finger-vein-based biometric identification,” *IEEE Trans. Inf. Forensics Security*, vol. 14, pp. 360–373, 2019.
- [15] M. Favre, S. Picard, J. Bringer, and H. Chabanne, “Balancing is the key: Performing finger vein template protection using fuzzy commitment,” in *Proc. 1st Int. Conf. Inf. Syst. Security Privacy*, 2015, pp. 304–311.
- [16] J. Feng and A. K. Jain, “FM model based fingerprint reconstruction from minutiae template,” in *Proc. Int. Conf. Biometrics*, 2009, pp. 544–553.
- [17] J. Feng and A. K. Jain, “Fingerprint reconstruction: From minutiae to phase,” *IEEE Trans. Pattern Anal. Mach. Intell.*, vol. 33, no. 2, pp. 209–223, Feb. 2011.
- [18] J. Galbally, A. Ross, M. Gomez-Barrero, J. Fierrez, and J. Ortega-Garcia, “Iris image reconstruction from binary templates: An efficient probabilistic approach based on genetic algorithms,” *Comput. Vis. Image Understand.*, vol. 117, no. 10, pp. 1512–1525, 2013.
- [19] M. Gomez-Barrero and J. Galbally, “Reversing the irreversible: A survey on inverse biometrics,” *Comput. Security*, vol. 90, Mar. 2020, Art. no. 101700.
- [20] M. Gomez-Barrero, J. Galbally, J. Fierrez, J. Ortega-Garcia, A. Morales, and M. A. Ferrer, “Inverse biometrics: A case study in hand geometry authentication,” in *Proc. 21st Int. Conf. Pattern Recognit. (ICPR)*, 2012, pp. 1281–1284.
- [21] I. Goodfellow *et al.*, “Generative adversarial networks,” *Commun. ACM*, vol. 63, no. 11, pp. 139–144, 2020.

- [22] D. Hartung and C. Busch, "Why vein recognition needs privacy protection," in *Proc. 5th Int. Conf. Intell. Inf. Hiding Multimedia Signal Process.*, 2009, pp. 1090–1095.
- [23] Z. He, W. Zuo, M. Kan, S. Shan, and X. Chen, "AttGAN: Facial attribute editing by only changing what you want," *IEEE Trans. Image Process.*, vol. 28, pp. 5464–5478, 2019.
- [24] B. Huang, Y. Dai, R. Li, D. Tang, and W. Li, "Finger-vein authentication based on wide line detector and pattern normalization," in *Proc. 20th Int. Conf. Pattern Recognit. (ICPR)*, 2010, pp. 1269–1272.
- [25] S. Iizuka, E. Simo-Serra, and H. Ishikawa, "Let there be color! Joint end-to-end learning of global and local image priors for automatic image colorization with simultaneous classification," *ACM Trans. Graph.*, vol. 35, no. 4, pp. 1–11, 2016.
- [26] P. Isola, J.-Y. Zhu, T. Zhou, and A. A. Efros, "Image-to-image translation with conditional adversarial networks," in *Proc. IEEE Conf. Comput. Vis. Pattern Recognit.*, 2017, pp. 1125–1134.
- [27] A. Jain, A. A. Ross, and K. Nandakumar, *Introduction to Biometrics*. Boston, MA, USA: Springer, 2011.
- [28] A. K. Jain, A. Ross, and U. Uludag, "Biometric template security: Challenges and solutions," in *Proc. 13th Eur. Signal Process. Conf.*, 2005, pp. 1–4.
- [29] R. Kabaciński and M. Kowalski, "Vein pattern database and benchmark results," *Electron. Lett.*, vol. 47, no. 20, pp. 1127–1128, 2011.
- [30] C. Kauba, S. Kirchgasser, V. Mirjalili, A. Ross, and A. Uhl, "Inverse biometrics: Reconstructing grayscale finger vein images from binary features," in *Proc. IAPR/IEEE Int. Joint Conf. Biometrics (IJCB)*, Houston, Texas, USA, 2020, pp. 1–8.
- [31] C. Kauba, B. Prommegger, and A. Uhl, "The two sides of the finger—An evaluation on the recognition performance of dorsal vs. palmar finger-veins," in *Proc. Int. Conf. Biometrics Spec. Interest Group (BIOSIG)*, Darmstadt, Germany, 2018, pp. 239–246.
- [32] C. Kauba, B. Prommegger, and A. Uhl, "Openvein—An open-source modular multipurpose finger vein scanner design," in *Handbook of Vascular Biometrics*, A. Uhl, C. Busch, S. Marcel, and R. Veldhuis, Eds. Cham, Switzerland: Springer, 2019, ch. 3, pp. 77–111.
- [33] C. Kauba and A. Uhl, "Shedding light on the veins—Reflected light or transillumination in hand-vein recognition," in *Proc. 11th IAPR/IEEE Int. Conf. Biometrics (ICB)*, Gold Coast QLD, Australia, 2018, pp. 1–8.
- [34] C. Kauba and A. Uhl, "An available open-source vein recognition framework," in *Handbook of Vascular Biometrics*, A. Uhl, C. Busch, S. Marcel, and R. Veldhuis, Eds. Cham, Switzerland: Springer, 2019, ch. 4, pp. 113–142.
- [35] S. Kirchgasser, C. Kauba, Y.-L. Lai, J. Zhe, and A. Uhl, "Finger vein template protection based on alignment-robust feature description and index-of-maximum hashing," *IEEE Trans. Biom., Behav., Ident. Sci.*, vol. 2, no. 4, pp. 337–349, Oct. 2020.
- [36] A. Kumar and Y. Zhou, "Human identification using finger images," *IEEE Trans. Image Process.*, vol. 21, pp. 2228–2244, 2012.
- [37] R. S. Kuzu, E. Picciuco, E. Maiorana, and P. Campisi, "On-the-fly finger-vein-based biometric recognition using deep neural networks," *IEEE Trans. Inf. Forensics Security*, vol. 15, pp. 2641–2654, 2020.
- [38] G. Larsson, M. Maire, and G. Shakhnarovich, "Learning representations for automatic colorization," in *Proc. Eur. Conf. Comput. Vis.*, 2016, pp. 577–593.
- [39] E. C. Lee, H. C. Lee, and K. R. Park, "Finger vein recognition using minutia-based alignment and local binary pattern-based feature extraction," *Int. J. Imag. Syst. Technol.*, vol. 19, no. 3, pp. 179–186, 2009.
- [40] J. Long, E. Shelhamer, and T. Darrell, "Fully convolutional networks for semantic segmentation," in *Proc. IEEE Conf. Comput. Vis. Pattern Recognit.*, 2015, pp. 3431–3440.
- [41] Y. Lu, S. J. Xie, S. Yoon, Z. Wang, and D. S. Park, "An available database for the research of finger vein recognition," in *Proc. 6th Int. Congr. Image Signal Process. (CISP)*, vol. 1, 2013, pp. 410–415.
- [42] G. Mai, K. Cao, P. C. Yuen, and A. K. Jain, "On the reconstruction of face images from deep face templates," *IEEE Trans. Pattern Anal. Mach. Intell.*, vol. 41, no. 5, pp. 1188–1202, May 2019.
- [43] S. K. Maji, H. M. Yahia, and H. Badri, "Reconstructing an image from its edge representation," *Digit. Signal Process.*, vol. 23, no. 6, pp. 1867–1876, 2013.
- [44] Y. Matsuda, N. Miura, A. Nagasaka, H. Kiyomizu, and T. Miyatake, "Finger-vein authentication based on deformation-tolerant feature-point matching," *Mach. Vis. Appl.*, vol. 27, no. 2, pp. 237–250, 2016.
- [45] N. Miura, A. Nagasaka, and T. Miyatake, "Extraction of finger-vein patterns using maximum curvature points in image profiles," *IEICE Trans. Inf. Syst.*, vol. 90, no. 8, pp. 1185–1194, 2007.
- [46] N. Miura, A. Nagasaka, and T. Miyatake, "Feature extraction of finger-vein patterns based on repeated line tracking and its application to personal identification," *Mach. Vis. Appl.*, vol. 15, no. 4, pp. 194–203, 2004.
- [47] V. M. Patel, N. K. Ratha, and R. Chellappa, "Cancelable biometrics: A review," *IEEE Signal Process. Mag.*, vol. 32, no. 5, pp. 54–65, Sep. 2015.
- [48] E. Picciuco, E. Maiorana, C. Kauba, A. Uhl, and P. Campisi, "Cancelable biometrics for finger vein recognition," in *Proc. 1st Int. Workshop Sens. Process. Learn. Intell. Mach. (SPLINE)*, 2016, pp. 1–5.
- [49] X. Qiu, W. Kang, S. Tian, W. Jia, and Z. Huang, "Finger vein presentation attack detection using total variation decomposition," *IEEE Trans. Inf. Forensics Security*, vol. 13, pp. 465–477, 2018.
- [50] C. Rathgeb and A. Uhl, "A survey on biometric cryptosystems and cancelable biometrics," *EURASIP J. Inf. Security*, vol. 2011, no. 3, Sep. 2011.
- [51] O. Ronneberger, P. Fischer, and T. Brox, "U-Net: Convolutional networks for biomedical image segmentation," in *Proc. Int. Conf. Med. Image Comput. Comput. Assist. Intervent.*, 2015, pp. 234–241.
- [52] A. Ross, J. Shah, and A. K. Jain, "From template to image: Reconstructing fingerprints from minutiae points," *IEEE Trans. Pattern Anal. Mach. Intell.*, vol. 29, no. 4, pp. 544–560, Apr. 2007.
- [53] A. A. Ross, J. Shah, and A. K. Jain, "Toward reconstructing fingerprints from minutiae points," in *Proc. Biometric Technol. Human Identification II*, vol. 5779, 2005, pp. 68–80.
- [54] A. F. Sequeira *et al.*, "PROTECT multimodal DB: A multimodal biometrics dataset envisaging border control," in *Proc. Int. Conf. Biometrics Spec. Interest Group (BIOSIG)*, Darmstadt, Germany, 2018, pp. 1–8.
- [55] J.-L. Starck, J. Fadili, and F. Murtagh, "The undecimated wavelet decomposition and its reconstruction," *IEEE Trans. Image Process.*, vol. 16, pp. 297–309, 2007.
- [56] P. Tome and S. Marcel, "On the vulnerability of palm vein recognition to spoofing attacks," in *Proc. Int. Conf. Biometrics (ICB)*, 2015, pp. 319–325.
- [57] P. Tome, M. Vanoni, and S. Marcel, "On the vulnerability of finger vein recognition to spoofing," in *Proc. Int. Conf. Biometrics Spec. Interest Group (BIOSIG)*, 2014, pp. 1–10.
- [58] P. Tome, M. Vanoni, and S. Marcel, "On the vulnerability of finger vein recognition to spoofing attacks," in *Proc. Int. Conf. Biometrics Spec. Interest Group (BIOSIG)*, Sep. 2014, pp. 111–120.
- [59] B. T. Ton and R. N. Veldhuis, "A high quality finger vascular pattern dataset collected using a custom designed capturing device," in *Proc. Int. Conf. Biometrics (ICB)*, 2013, pp. 1–5.
- [60] A. Uhl, C. Busch, S. Marcel, and R. Veldhuis, *Handbook of Vascular Biometrics (Advances in Computer Vision and Pattern Recognition)*. Cham, Switzerland: Springer, 2019.
- [61] S. Venugopalan and M. Savvides, "How to generate spoofed irises from an iris code template," *IEEE Trans. Inf. Forensics Security*, vol. 6, pp. 385–395, 2011.
- [62] T.-C. Wang, M.-Y. Liu, J.-Y. Zhu, A. Tao, J. Kautz, and B. Catanzaro, "High-resolution image synthesis and semantic manipulation with conditional gans," in *Proc. IEEE Conf. Comput. Vis. Pattern Recognit.*, 2018, pp. 8798–8807.
- [63] X. Yan, J. Yang, K. Sohn, and H. Lee, "Attribute2Image: Conditional image generation from visual attributes," in *Proc. Eur. Conf. Comput. Vis.*, 2016, pp. 776–791.
- [64] W. Yang *et al.*, "Securing mobile healthcare data: A smart card based cancelable finger-vein bio-cryptosystem," *IEEE Access*, vol. 6, pp. 36939–36947, 2018.
- [65] Y. Yin, L. Liu, and X. Sun, "SDUMLA-HMT: A multimodal biometric database," in *Proc. Chin. Conf. Biometric Recognit.*, 2011, pp. 260–268.
- [66] J. Zhang and J. Yang, "Finger-vein image enhancement based on combination of gray-level grouping and circular gabor filter," in *Proc. Int. Conf. Inf. Eng. Comput. Sci.*, 2009, pp. 1–4.
- [67] J. Zhao, H. Tian, W. Xu, and X. Li, "A new approach to hand vein image enhancement," in *Proc. 2nd Int. Conf. Intell. Comput. Technol. Autom.*, vol. 1, 2009, pp. 499–501.
- [68] J.-Y. Zhu, T. Park, P. Isola, and A. A. Efros, "Unpaired image-to-image translation using cycle-consistent adversarial networks," in *Proc. IEEE Int. Conf. Comput. Vis.*, 2017, pp. 2223–2232.
- [69] K. Zuiderveld, "Contrast limited adaptive histogram equalization," in *Graphics Gems IV*. London, U.K.: Academic, 1994, pp. 474–485.



Christof Kauba received the B.Eng. and M.Sc. degrees and the Ph.D. degree in applied information technology from the University of Salzburg, Austria, in 2013, 2015, and 2018, respectively, where he is a Postdoctoral Researcher with the Department of Computer Sciences. His research interests include image and video processing, image forensics and biometrics, especially biometric sensor design as well as finger- and hand vein biometrics.



Andreas Uhl (Senior Member, IEEE) is a Professor with the Department of Computer Sciences, University of Salzburg, where he heads the Multimedia Processing and Security Lab. His research interests include image and video processing and compression, wavelets, media security, medical imaging, biometrics, and number-theoretical numerics.



Simon Kirchgasser received the M.Sc. degree in applied image and signal processing from the University of Salzburg and University of Applied Sciences Salzburg in 2016. He is currently pursuing the Ph.D. degree with the Department of Computer Sciences, University of Salzburg, where he is working as a Research Assistant. His main research interest is in fingerprint and vascular biometrics, especially focusing on the influence of varying acquisition conditions as well as ageing aspects in fingerprint biometrics and template protection in vascular biometrics.



Arun Ross (Senior Member, IEEE) received the B.E. degree (Hons.) in computer science from BITS Pilani, India, and the M.S. and Ph.D. degree in computer science and engineering from Michigan State University, where he is the John and Eva Cillag Endowed Chair with the College of Engineering and a Professor with the Department of Computer Science and Engineering. He was with the Faculty of West Virginia University from 2003 to 2012. His expertise is in the area of biometrics, computer vision, and machine learning. He received the

Benedum Distinguished Scholar Award for excellence in creative research and the WVU Foundation Outstanding Teaching Award from West Virginia University. He is a recipient of the NSF CAREER Award and was designated a Kavli Fellow by the U.S. National Academy of Sciences by virtue of his presentation at the 2006 Kavli Frontiers of Science Symposia. In recognition of his contributions to the field of pattern recognition and biometrics, he received the JK Aggarwal Prize in 2014 and the Young Biometrics Investigator Award in 2013 from the International Association of Pattern Recognition. He has advocated for the responsible use of biometrics in multiple forums, including the NATO Advanced Research Workshop on Identity and Security in Switzerland in 2018. He testified as an Expert Panelist in an event organized by the United Nations Counter-Terrorism Committee at the UN Headquarters in 2013.



Vahid Mirjalili received the Ph.D. degree in computer science and engineering from the Michigan State University. During his Ph.D. in computer science, he worked with iProBe lab, where he focused his research efforts on applications of machine learning and deep learning in the domain of computer vision.